PROCEEDINGS OF SPIE

SPIEDigitalLibrary.org/conference-proceedings-of-spie

Characterization facility for the MAJIS/JUICE VIS-NIR FM and SM detectors

Bolsee, David, Van Laeken, Lionel, Cisneros-González, Miriam, Pereira, Nuno, Depiesse, Cédric, et al.

David Bolsee, Lionel Van Laeken, Miriam E. Cisneros-González, Nuno Pereira, Cédric Depiesse, Lars Jacobs, Ann Carine Vandaele, Birgit Ritter, Samuel Gissot, Özgür Karatekin, François Poulet, Yves Langevin, Cydalise Dumesnil, Jean-Pierre Dubois, Antoine Arondel, Paolo Haffoud, Christian Ketchazo, Véronique Hervier, "Characterization facility for the MAJIS/JUICE VIS-NIR FM and SM detectors," Proc. SPIE 11443, Space Telescopes and Instrumentation 2020: Optical, Infrared, and Millimeter Wave, 114437H (13 December 2020); doi: 10.1117/12.2576319

SPIE.

Event: SPIE Astronomical Telescopes + Instrumentation, 2020, Online Only

Characterization facility for the MAJIS/JUICE VIS-NIR FM and SM detectors

David Bolsée[a], Lionel Van Laeken[a], Miriam E. Cisneros-González[b], Nuno Pereira[a], Cédric Depiesse[a], Lars Jacobs[a], Ann C. Vandaele[a], Birgit Ritter[c], Samuel Gissot[c], Özgür Karatekin[c], François Poulet[d], Yves Langevin[d], Cydalise Dumesnil[d], Jean Pierre Dubois[d], Antoine Arondel[d], Paolo Haffoud[d], Christian Ketchazo[d], and Veronique Hervier[d]

[a]Royal Belgian Institute for Space Aeronomy (BIRA-IASB), 1180 Brussels, Belgium
[a]Institute of Condensed Matter and Nanosciences, Université catholique de Louvain, B-1348 Louvain-la-Neuve, Belgium
[c]Royal Observatory of Belgium (ROB), 1180 Brussels, Belgium
[d]Institute of Space Astrophysics (IAS), 91440 Bures-sur-Yvette, France

ABSTRACT

MAJIS is part of the science payload of the ESA L-Class mission JUICE to be launched in 2022 with an arrival at Jupiter in 2030. MAJIS will perform imaging spectroscopy through two channels: VIS-NIR (0.50 µm - 2.35 µm) and IR (2.25 µm - 5.54 µm). The Royal Belgian Institute for Space Aeronomy (BIRA-IASB) and the Royal Observatory of Belgium (ROB) contribute to MAJIS with the characterization and calibration of the VIS-NIR Flight Model (FM) and Spare Model (SM) detectors, including the design, development, and validation of the setup, as well as the data processing pipeline. The FM and SM detectors are characterized under different illumination conditions (along four decades of dynamical range), temperature (125 K – 144 K), beam uniformities, exposure times, and/or data acquisition rates. In this paper, we describe the optical performances of the facility, which can be configurable for dark conditions, uniform light beam, and convergent beam with same focal ratio as MAJIS convergence optics. We provide a relative radiometry scale for the typical characterization measurements, as well as a fully characterized flux that will allow us to perform characterization measurements in an absolute radiometry scale, such as quantum efficiency (QE). In addition, we describe the thermal performances provided by the bench reaching different temperature scenarios, including the expected operating temperature of the detector at 132 K. The characterization facility was completed and subjected to validation tests in early 2020. The MAJIS VIS-NIR FM detector was delivered for its complete characterization in June 2020.

Keywords: JUICE, MAJIS, VIS-NIR detectors, detectors characterization, imaging spectroscopy, absolute radiometry, quantum efficiency, electro-optic characterization

1. INTRODUCTION

BIRA-IASB and ROB institutes (called 'Spacepole' in this paper) have more than thirty years of experience in the development and the characterization of payloads for space projects, within national and international consortiums. The experiments are mainly designed for research in solar physics (LYRA[1], EUI[2], SOLSPEC[3]) and planetology (SOIR[4], NOMAD[5]) with a spectral range extending from Extreme Ultraviolet (EUV) to Infrared (IR). These instrumentations can be developed for (i) absolute radiometry to perform solar direct irradiance measurements (by using spectro- or filter- radiometers), and (ii) spectral imaging and spectroscopy for the study of solar disk features or to investigate the composition of planetary atmospheres and their trace species. For any instrumentation developed there is a need to perform a full pre-flight characterization, especially for those designed for space missions and facing harsh vacuum, thermal and radiative environment. Indeed, at the instrument and its detector level, measurement equations and transfer functions are used to convert raw electronic signals into meaningful and useful scientific data. All the parameters appearing in these equations

Further author information:
D.B.: E-mail: david.bolsee@aeronomie.be, Phone: +32 (0)2 373 03 51

Space Telescopes and Instrumentation 2020: Optical, Infrared, and Millimeter Wave, edited by Makenzie Lystrup, Marshall D. Perrin, Proc. of SPIE Vol. 11443, 114437H · © 2020 SPIE
CCC code: 0277-786X/20/$21 · doi: 10.1117/12.2576319

must be characterized. For example, dark and saturation levels, correction factors for non-linearity, temperature dependencies, or angular response within the field of view, must be established. If required, radiometric and wavelength calibration must be performed to have built-in response curves. Another reason of characterization is the need to verify if the design is valid for flight conditions. Ideally, the design should include internal units for aging monitoring and trend corrections if post-flight calibration is not possible. The transfer functions provide also the key relationship to derive the uncertainty of any single measurement.

One example developed in this paper is the Spacepole involvement for the full characterization of one subsystem of the MAJIS[6] (Moons And Jupiter Imaging Spectrometer) instrument. MAJIS is one of the key science instruments of the JUICE (Jupiter Icy Moons Explorer) payload. The JUICE spacecraft, developed within the ESA Cosmic Vision Program 2015-2025, will be launched in 2022 and will arrive near Jupiter in 2030 after several flybys of Earth, Venus and Mars. This mission will perform for at least three years, detailed observations of the whole Jovian system[7] through a spectral characterization to increase our knowledge. The main scientific objectives are summarized as: (i) study of the Jupiter's atmosphere (structure, dynamics and composition) and magnetosphere (including aurora), (ii) study of the surfaces and exospheres of the Jupiter's satellites (with particular emphasis on Ganymede and including the moon's interactions with the Jupiter's magnetosphere).

MAJIS is a hyper-spectral imaging spectrometer with two different channels: VIS-NIR (0.5 µm – 2.35 µm) and IR (2.25 µm – 5.54 µm), suitable to address most of the JUICE mission's scientific goals[8]. The design and integration of MAJIS is in charge of IAS (Institut d'Astrophysique Spatiale, France) and LDO (Leonardo S.p.A, Italy). The matrix detectors for both channels are the H1RG^{TM} devices (HgCdTe array[9] of 1024 × 1024 pixels) from Teledyne Technologies Inc. (USA). At instrument level, each detector is integrated in one enclosure defined as the Focal Plane Unit (FPU). This module (Figure 1) guarantees the nominal cleanliness, thermalization, straylight rejection and optical alignment of the FPU internal components. These are: (i) the Focal Plane Array (FPA) detector, (ii) the Focal Plane Electronics (FPE), (iii) the thermo-mechanical assembly (FPAssy), (iv) the Linear Variable Filter (LVF, namely for high diffraction order rejection), and (v) the internal flex cable (FPF) to read-out the detector and its thermometry from the FPE. Additional harnesses read-out the amplified signals to the Secure Access Module (SAM) card, which works at room environment as an interface between the FPU and its Ground Support Equipment (FPU-GSE) system, where the image acquisition is controlled.

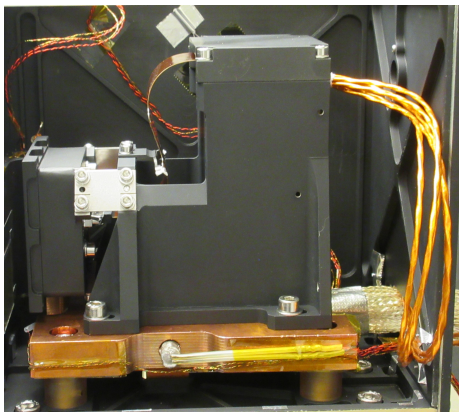

Figure 1. General view of the MAJIS VIS-NIR FPU as integrated in the facility.

The Spacepole involvement on the MAJIS project is to complete the full electro-optic characterization in dark and under illumination conditions of the spare (SM) and flight (FM) models of the VIS-NIR detector. In that way, the detector performances (as stated by the Teledyne company) can be verified in detail. Moreover, thanks to the simulated in-flight environment in the laboratory facility, it contributed (at the detector level) to the determination of the VIS-NIR channel transfer function and helped for the study of the mission predictions. This work was done within a consortium with IAS, and supervised by CNES (Centre National d'Etudes Spatiales, France) and the Belgian User Support and Operations Center (B.USOC). At Spacepole side, the Space optoelectronic and optical Technology and Calibration Laboratory (STCL) was involved with the support of the

BIRA-IASB engineering department. STCL is a joint structure between BIRA-IASB and ROB whose purpose is to provide facilities and expertise, namely to support the characterization of sub-systems for space instrumentation. The STCL is equipped with different existing facilities, but joint efforts were required to develop a new, high-performances and safe thermal-vacuum facility especially dedicated to the MAJIS VIS-NIR detector characterization. The main topic of this paper is to describe in detail the design and operational mode of this VIS-NIR facility, but also to demonstrate its flexible and versatile operational mode to characterize other sub-systems or whole instruments for future projects. The description of the security system developed for the characterization facility is available[10], as well as the results of the FM MAJIS VIS-NIR detector characterization[11].

2. VIS-NIR CHARACTERIZATION FACILITY

The full characterization of an array detector response corresponds to a wide panel of tests. For its response under light conditions, it must cover the range from complete dark to maximum response, i.e. from Dark Current (DC) to the Full-Well Capacity (FWC) and saturation. In this range, any deviation from an ideal linear response must be characterized (linearity in function of integration time and the flux) as well as the uniform response of the matrix of pixels, with or without light, which is the case for Dark Signal Non-Uniformity (DSNU), Photo-Response Non-Uniformity (PRNU), the identification of defective clusters, and the operability of every pixel. Moreover, the useful spectral range between the cut-on and cut-off as well as the Quantum Efficiency (QE) are key parameters. Likewise, there are behaviors related to the electronics that must be measured, such as the bias, Read-Out Noise (RON), gain and latency. Finally, one specific task for MAJIS is the measurement of the LVF alignment in the FPA. All parameters can be intrinsically dependent on Integration Time (IT), flux level and wavelength. In addition, the whole range of temperatures corresponding to the mission conditions must be scanned. These measurements define the full scope of a characterization campaign[11], so the facility must be designed and validated in that sense.

2.1 Fundamentals of the VIS-NIR facility

The VIS-NIR facility is installed in the BIRA-IASB laboratory. The detectors must be characterized under high-vacuum, for FPA operative temperature ranging from 116 K to 160 K, with the FPE operating above 120 K to avoid irreparable damage[12]. Therefore, a vacuum chamber (VC) combined with a cryocooler system is required. For illumination conditions, an optical bench is installed close to the VC. These equipment (described below) are installed under a laminar flux that meets the ISO-5 cleanliness requirement to expose the MAJIS FM and SM detectors[12]. A contiguous ISO-7 room, acting as an airlock of the ISO-5 area, is used for different handling procedures and for the installation of all electronic devices for remote control of the facility (controllers, electrometers). In that way, the human operations are limited in the ISO-5 area, for safety reasons, except during the installation and uninstallation of the detectors. An additional control room is available for the Optical Ground Support Equipment (OGSE) and Temperature Ground Support Equipment (TGSE) systems, where the personnel can remotely operate the facility. Environmental parameters as the pressure, oxygen concentration, ambient temperature and relative humidity at the ISO-5 and ISO-7 areas, are continuously monitored. The Product and Quality Assurance (PA/QA) is ensured by BIRA-IASB (B.USOC).

2.2 Thermal-vacuum system

The High-Vacuum Chamber is the customized cubical model TRINOS DN-750 (volume of 420 L) from Pfeiffer Vacuum[13]. It is used to simulate the flight conditions and to reduce the thermal transfer between the internal components, during the cryogenic cooling of the MAJIS detectors. This VC is equipped with various flanges for the cabling interfaces (harness and wires) required for the FPU operations, and thermometry elements to conduct a typical characterization campaign under cryogenic conditions. The VC includes a CaF_2 viewport (63 mm of diameter) for internal photon flux illumination when required. Additional flanges are used for the vacuum and cooling equipment. The required vacuum level to simulate space conditions and achieve the expected low temperatures without any risk of contamination in the detectors, is lower than 10^{-5} mbar. This high vacuum level is achieved by using a turbo pump (Pfeiffer HiPace 300 H[14]) coupled with a dry pump (Pfeiffer ACP 15[15]). Although a vacuum level of about 1×10^{-5} mbar can be achieved in 80 minutes, the ultimate vacuum level observed with all sub-system under test and associated equipment inside the VC is in the order of 10^{-7} mbar.

The pumping system is provided with customized and factory-designed interfaces to monitor its operating status and take action in case of issue. The TGSE is continuously monitoring the vacuum level of the VC, by two pressure gauges[16,17] (one redundant), whose controllers provide output relays that can be configured for the control of threshold vacuum levels. These threshold levels are used to coordinate the activation of elements that constitute the cryogenic/pumping system, and for leak detection. Additionally, two calibrated pressure relief valves (one redundant) open to prevent issue in case of overpressure during venting operations. Finally, two normally-closed safety valves protect the sensitive equipment inside the VC against abrupt vacuum loss induced by any vacuum system failure. The main valve, downstream the turbo pump, isolates the VC in case of leaks. A secondary valve isolates the dry pump if it stops working. All output signals related to the pumps operation status, the vacuum level and the valves, are managed by the security system of the facility[10] to prevent damage and contamination of the sensitive FM payload. The venting of the VC, when required, is performed using high grade (5.0) Nitrogen. The diagram of the vacuum system is presented in Figure 2.

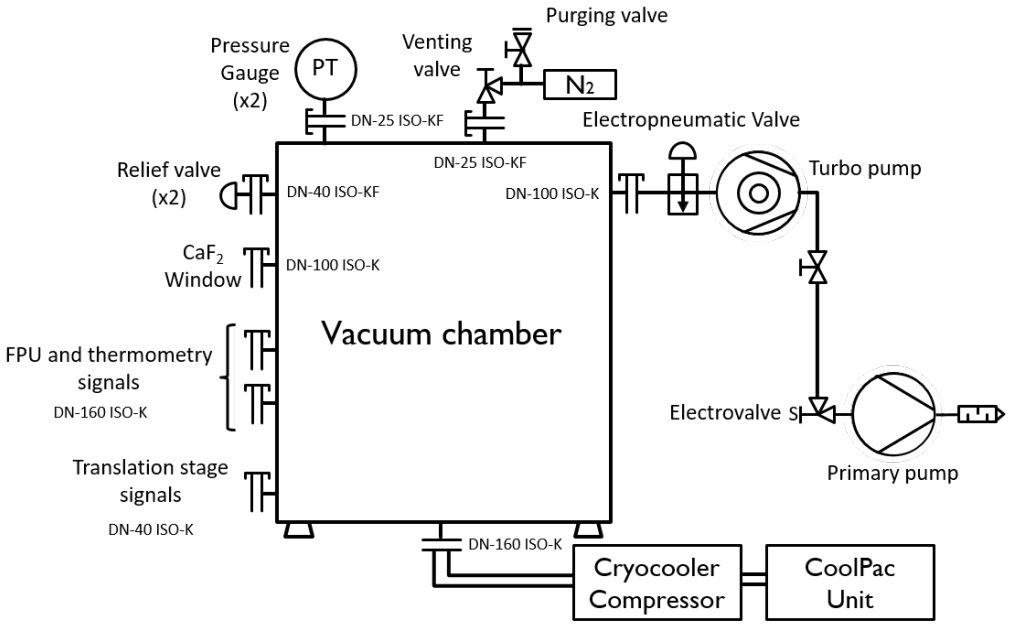

Figure 2. General vacuum diagram of the MAJIS VIS-NIR characterization facility.

To provide the necessary thermal conditions for the FPU characterization procedures, the close-cycle cryocooler system[18] is implemented in the facility through one flange of the VC. It provides a cooling power of 60 W at 77 K, with ultimate performance of 25 K without load. The cold head is thermally connected to the payload by means of a rigid Oxygen Free High-Conductivity (OFHC) copper thermal link. In this way, the minimum cooling temperature achieved to thermalize a sub-system under test by using this facility, is around 95 K. A special enclosure (radiation shield) was designed to: (i) thermalize the payload at any required low temperature, and (ii) prevent it from outside straylight contamination, especially from NIR wavelengths. The straylight is not limited to photons coming from the viewport, but also from thermal emission (blackbody radiation) emerging from all surfaces and items at room temperature, or warmer enough to produce parasite radiation inside the VC. If the detector under test is sensitive for wavelengths larger than 1.5 μm, this emission will be detected as straylight. Consequently, a radiation shield was designed as a vacuum-compatible cold box, externally covered by MLI.

The FPU mount developed for the MAJIS VIS-NIR project follows the fundamentals described above (Figure 3). The main parts of the FPU mount are a radiation shield, a movable cold plate and a copper base plate. The radiation shield corresponds to the mentioned enclosure box, with one aperture in the frontal panel to allow incoming photon flux along the optical path for the detector illumination. Options to characterize in dark and light conditions are offered by the movable plate with positions: open, close or filter (to better control the

straylight). One requirement to avoid straylight from thermal emitters on a VIS-NIR H1RG^{TM} MAJIS detector, is to maintain the radiation shield and movable plate at a temperature below 172 K[19]. The copper base plate receives the payload to thermalize it, since the survival line of the MAJIS VIS-NIR FPU, which contains heaters and additional temperature sensors, is not intended to be used during the characterization[12].

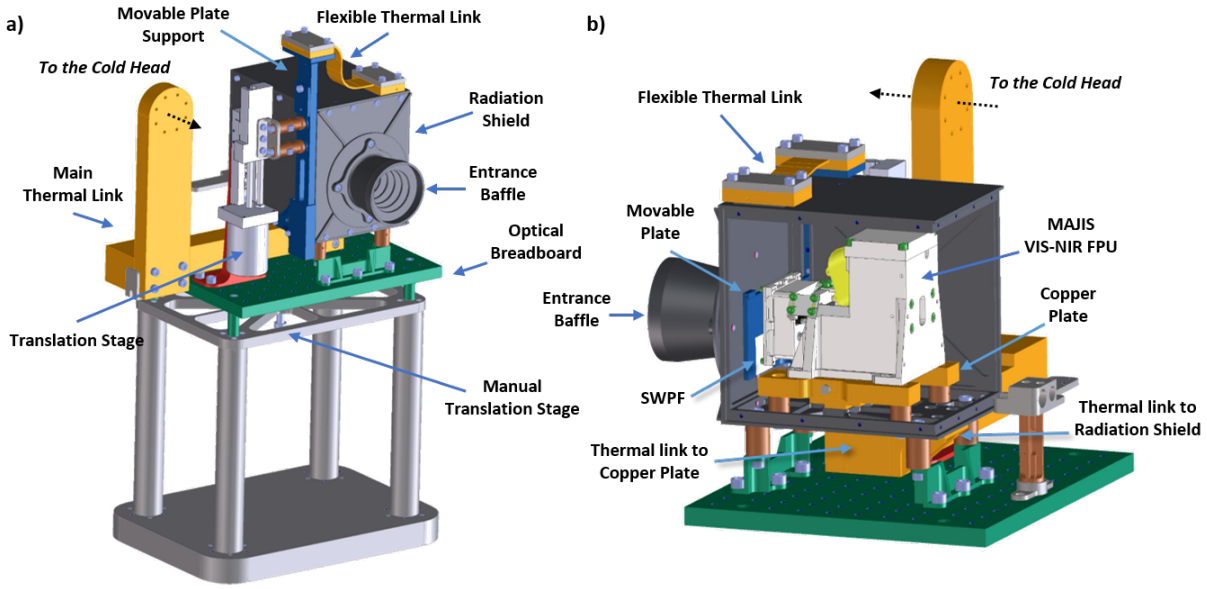

Figure 3. The FPU mount developed to support and thermalize the MAJIS VIS-NIR detector: a) Frontal view, b) internal view of the radiation shield. The optical breadboard (at room temperature) is mounted on a translation system for optical alignment.

The FPU mount provides an assembly of secondary parts that contributes to the thermalization. These parts of different sizes and materials where carefully chosen for insulation (decoupling of room temperatures and different cold stages) and conduction. Figure 4 shows the complete thermal lumped scheme of the FPU mount. The Oxygen-Free High Conductivity (OFHC) copper was the main conductive material used in the FPU mount although Aluminum 6082 was used for most of the parts with indium foils to improve the mechanical contact between components. Several flexible straps were used to thermalize the movable plate inside the radiation shield. For insulation, PEI-Ultem^{TM} 1000 was chosen due to its low conductivity (0.24 W/m K)[20]. All materials used for the mount are compliant with the outgassing requirements: Total Mass Lost (TML) < 1 % and Collected Volatile Condensable Materials (CVCM) < 0.1 %[12].

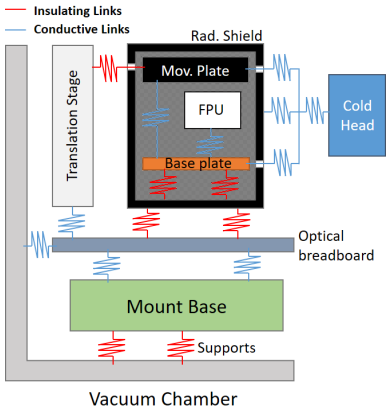

Figure 4. Thermal lumped scheme of the FPU mount.

The fine thermal regulation of the the elements in the FPU mount (including the copper base plate, the cold head of the cryocooler, the movable plate and the translation stage) is obtained by means of PID control loops managed by LakeShore temperature controllers[21,22] provided with calibrated PT100 temperature sensors and heaters. The TGSE system is continuously monitoring the functioning of the temperature control loops and the temperature at the different elements of the mount. The temperature controllers are configured to activate alarms when the temperature in a specific element is outside the specified safe range to prevent damage on critical devices, especially the MAJIS VIS-NIR FPU. The settings of these alarms and corresponding actions (for example, interruption of the cooling cycle) are managed by the TGSE and the security system[10] of the facility. Although the FPU mount was especially designed for the MAJIS project, the functioning principle is similar for each VIS-NIR characterization and can be applied for future characterization projects. Therefore, the payload enclosure can be adapted in a flexible and versatile way to meet other measurement plans.

2.3 Specifications for the optical system

The optical equipment for radiometry of the VIS-NIR facility is installed on an optical table contiguous to the VC (Figure 5). It is used only for payload characterization under illumination. For dark measurements, the movable cold plate inside the VC is simply configured in close position.

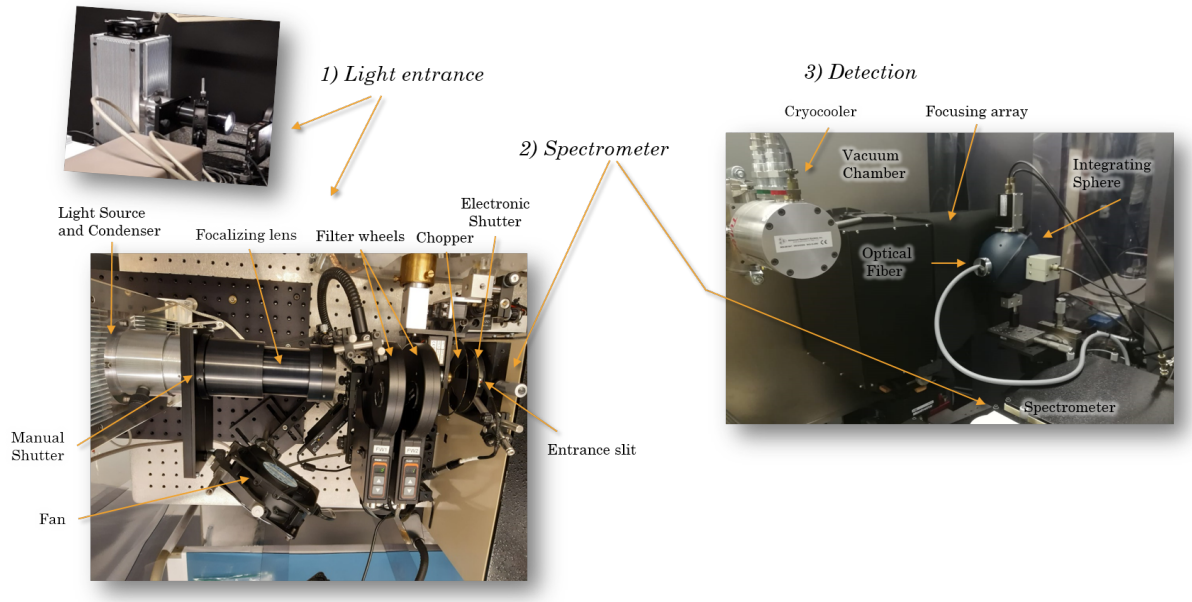

Figure 5. Opto-mechanical equipment of the MAJIS VIS-NIR facility: 1) light entrance, 2) spectrometer, and 3) detection blocks.

To fulfill the characterization tasks in light conditions, the ideal specifications are the following[12]:

1. To provide a monochromatic, tunable and stable light of adjustable bandpass combined to the possibility of broadband (stable) illumination.
2. To provide adjustable levels of illumination, well calibrated for relative changes.
3. To allow homogeneous illumination in the plane of the detector under test, or within the FOV if a whole instrument is tested.
4. To perform absolute radiometry on a target plane inside the VC. It can be the FPA plane or the first active optical surface of the entrance optics of a whole instrument.
5. To offer on/off fast switching of the photon flux for latency measurements.
6. For MAJIS: to simulate the beam convergence of $\sim 11^\circ$ on the detector, as encountered by design in the FM of the MAJIS VIS-NIR spectro-imager for the dispersed light.

The facility was developed to meet these six requirements for the MAJIS project, except that only monochromatic illumination was necessary. An upgrade could easily be implemented to broadband or polychromatic illumination for other projects. For MAJIS, all optical equipment to configure the radiance was installed outside the VC. The main reason is the need of a direct control of the optical equipment and associated electronics during the bench validation and FM campaigns. The price to be paid was a current limitation in VIS and NIR spectral ranges and not for IR. It also justifies the use of a viewport to reach the detector with a photon flux.

The six specifications listed above require a well-developed opto-mechanical bench. It is organized in three main blocks as follows:

- **Light entrance**: for the light source and associated equipment to adjust the intensity and injection of the light irradiance into the spectrometer.
- **Spectrometer**: to provide the monochromatic light beam and its possible modulation.
- **Detection**: for the radiometry.

The interconnections between the opto-mechanical equipment and specifications are developed in Figure 6. The optical path is flushed by nitrogen during the characterization to avoid the water vapor absorption.

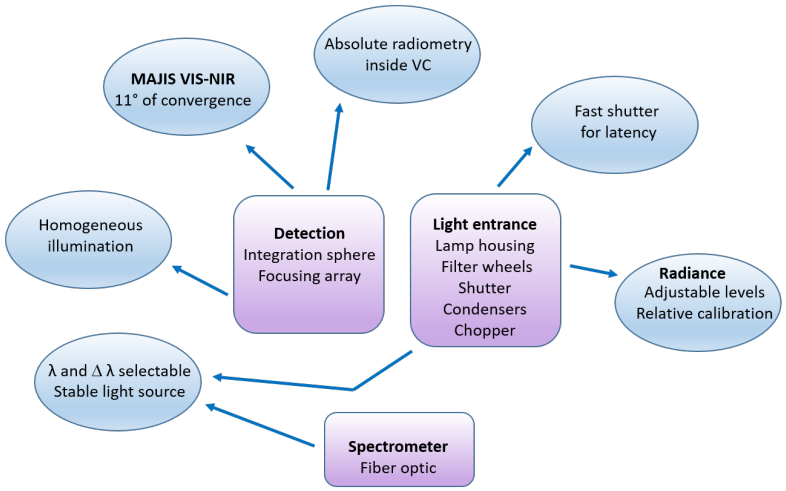

Figure 6. Interconnections between the opto-mechanical equipment of the facility and the performances specifications.

2.4 Light entrance and spectrometer system

The monochromatic and tunable light beam is obtained by the combination of a QTH 1000 W lamp[23] and a double monochromator. The lamp is supplied in continuous current mode at 8 A, stabilized at 10^{-3} % using a HP 6675A power supply[24]. Consequently, the radiance stability is about 0.1 %. The lamp is integrated and aligned in a lamp housing[25] equipped with an infrasil condenser for the beam collimation. The light injection through the entrance slit of the spectrometer is then optimized using an infrasil focalizing lens. The light entrance block is also completed with three main devices. First, a chopper[26] for the light modulation: the light is modulated in front of the entrance slit, only on request, when a PbS photodiode is used in the detection block. The entire chopper unit is mounted on an actuator, so that the blades can be aligned on or off the optical path to modulate or not the light. Secondly, an electronic shutter[27] with fast closing time (40 ms) is inserted in front of the entrance slit. In addition to DC measurement, its main task is to allow latency studies of the detector under test. The third device is the system to adjust the level of illumination. It simply consists in a combination of two 6-positions filter wheels equipped with neutral density filters with well-distributed optical densities. The combination of the different filters allows reaching up to 30 different levels of attenuation over four orders of magnitude.

The intensity of the lamp housing output is continuously monitored at a first stage, before the spectrometer, by using a multi-channels filter radiometer[28] with a moderate bandwidth of ∼10 nm. Helpful check is performed

for four peak wavelengths centered on 613 nm, 672 nm, 869 nm and 941 nm. This monitoring system is redundant to the function of the detection block.

The spectrometer used is the model DTMc300 from Bentham Instruments Ltd[29] and consists in a double monochromator. A high spectral purity, with straylight rejection of about 10^{-8}, can be achieved. The slits are manually adjusted to tune the bandpass to the required settings. Each monochromator is equipped with a turret that harbors three plane gratings with different grooves per mm (1200, 600, 300). Depending on the grating efficiency, the switch from gratings 1 to 2 and gratings 2 to 3 is optimized and occurs at 1100 nm and 2240 nm, respectively.

2.5 Signal detection and relative radiometry

The high homogeneity of monochromatic radiance after the transfer through the spectrometer is ideally produced by an Integrating Sphere (IS) that provides a lambertian source at its output port. The one integrated in the facility is a LabSphere model[30] of four-ports and 5.3 inch of diameter. Diameters of the ports are one inch, except the output port (2.5 inch). For flexibility reason of the optical mounting, it was decided to interface the IS and the spectrometer by means of a one meter long IR fiber optic[31]. Even if the IS and the fiber induce light attenuation, the use of a 1 kW QTH lamp provides enough photon flux for the payload characterization inside the VC. Two ports are available and used by a set of VIS-NIR photodiodes to perform radiance stability monitoring, and relative and absolute radiometry. For radiance stability and relative scales (typically to demonstrate a constant signal during frame acquisition, or to calibrate the level of illuminations for linearity in function of the flux), the signal is simply recorded at the IS level in arbitrary units. Absolute radiometry is more complex (see Section 2.7).

Concerning the photodiodes, four kind of receivers are available at the facility: Si[32], Ge[33], PbS[34] and InGaAs[35]. All receiver's cases are enclosed in a photodiodes mount. The size of the receiving area differs from one to another. In addition, the distance between these receivers and the housing of the photodiodes corresponds to the mechanical backfocale. The target spectral range for the MAJIS VIS-NIR project is 0.4 µm - 2.65 µm, for particular characterizations as the useful spectral range of the FPA. All photodiodes are sensitive at least from 400 nm. However, it is known that the Si spectral response is limited to approximately 1.25 µm while the Ge presents a cut-off around 1.8 µm. PbS and InGaAs cover the whole VIS-NIR spectral range. For the signal detection, the facility is equipped with different controllers: dataloggers[36] to read output signals in volts (V), picoammeters[37] to read photocurrents in amperes (A), or a Lock-in amplifier[38] combined with a preamplifier[39] to proceed to phase sensitive detection. The InGaAs is equipped with a proximity electronics (preamplifier) that converts its photocurrent in volts. Therefore, the signal is read-out directly in volts. The Si and Ge photodiodes provide output signals in amperes. For this set of Si, Ge, InGaAS detectors, their respective controllers are used. They can be operated with or without light modulation. In case of modulation, the signal is simply reduced by a factor of two by averaging on the integration time, due to chopper blades effect. The PbS photodiode needs to be operated by using a Lock-in amplifier. In that case, the rectified output signal is V_{rms}. It is worth to mention that the other photodiodes can also be connected to the Lock-in for the read-out. The rms factor is in that case specific to each detector. By design, it was expected to offer a versatile detection system and detector set, to meet the radiometric requirements for each selected wavelength (fine measurements for stability and level changes), and this objective is fulfilled.

2.6 Configurations for the VC interfaces

Two optical configurations (diffuse and converging) are designed to uniformly illuminate the payload in a working plan inside the VC (the FPA plane of the VIS-NIR MAJIS detector for instance). For diffuse and homogeneous illumination, the IS is directly connected to the viewport of the VC. To create a converging beam, a focusing array based on two off-axis concave mirrors and one aperture must be interfaced between the IS and the viewport. This array was optically designed by the Lambda-X company[40], and assembled at BIRA-IASB to provide the appropriate beam convergence (11° in average) that the MAJIS detector should receive after its integration at instrument level. These configurations are summarized in Figure 7.

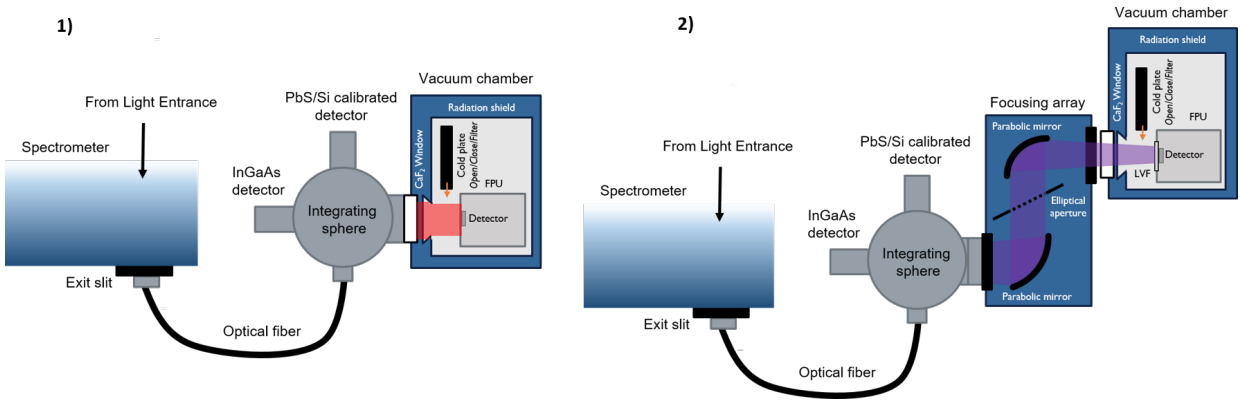

Figure 7. Configurations provided for a payload characterization (the MAJIS VIS-NIR FPU for instance): 1) uniform diffuse light beam, 2) uniform converging beam.

2.7 Methodology for absolute radiometry

The most important parameter for absolute radiometry in the working plan is the determination of the spectral power (W) that reaches each surface element dA for each wavelength. It was demonstrated that the absolute radiometry can only be experimentally performed at the IS level. Absolute calibrated photodiodes must be used for that purpose. The transfer and extinction of the spectral power along the remaining optical path, between the IS and the working plan (including a focusing array if required) is characterized by a function, whose parameters were experimentally measured during the validation campaign of the facility. This dimensionless transfer function R_0 describes the ratio of available spectral power between one reference (dA) of the working plane (WP) and one reference port of the IS (Equation 1).

$$R_0 = \frac{S_{IS}}{S_{WP}} \tag{1}$$

The term S_{IS} and S_{WP} are, respectively, the net signal of the photodiode used to build the transfer function. The reference surface element dA must be identified and positioned in a reproducible way. This lead to the definition of the optical axis of the facility, that corresponds to the line orthogonal to the center of the viewport of the VC. In 'diffuse light' configuration, the IS is connected to the viewport by means of a mechanical interface offering straylight rejection and accurate alignment on the optical axis. For the configuration 'converging beam', the focusing array is aligned on the viewport, at the appropriate distance between the second mirror and this window. The full performances of the focusing array are only met if the IS (whose output port being reduced to one inch of diameter) is accurately aligned on the optical axis of the first mirror, at a right distance. One optical mount with six degrees of freedom and different procedures were prepared to proceed to this alignment with success. Inside the VC, the intersection point between the working area and the optical axis defines the position of dA.

For both configurations, the transfer function R_0 was built during the MAJIS radiometric validation campaign for the MAJIS project (see Section 3.1). Results are presented in Figure 9.

One important point is that the illumination of the working plane, even if provided by the IS output, is not fully homogeneous. Consequently, the estimation of the spectral power for any surface element implies the application of a second characterization function that describes the illumination inhomogeneity. It is defined as the propagation function $H(x, y, \lambda)$, normalized at the position dA, referring the illumination intensity at this position. This function is used as a multiplicative factor to provide the required spectral power in any position, and it must be determined for both configurations and all wavelengths, as described in Equation 2. $P_{IS}(\lambda)$ is the spectral power measured at the IS level using calibrated photodiodes.

$$P(x, y, \lambda) = P_{IS}(\lambda)\ R_0(\lambda)\ H(x, y, \lambda) \tag{2}$$

Absolute radiometry applied to the MAJIS VIS-NIR detector for QE measurements is only possible if this detector is also aligned on the optical axis. The FPA pixel located at the intersection of the optical axis must be determined during a pre-campaign, to accurately propagate the spectral power received by each pixel. The function $H(x, y, \lambda)$ is then used as a multiplication factor. To measure the spectral power at IS level, the facility is equipped with a Si PTB (Physikalisch-Technische Bundesanstalt) calibrated photodiode[41] (spectral range 400 nm – 1100 nm), and an absolute calibrated PbS photodiode (spectral range 1000 nm – 3000 nm, whose Bentham calibration was reinforced up to 1.8 µm using a Ge PTB calibrated photodiode[42]). The calibration certificates provide the spectral power responsivity in A/W. Referring to Section 2.5, the PbS photocurrent is obtained from the V_{RMS} output signal of the Lock-in, then converted in ampere, knowing the RMS factor to be used for the PbS and the gain of the Lock-in preamplifier. If the picoammeter is used, for the Si photodiode, the photocurrent is directly obtained.

It is worth to mention that the propagation function that characterizes the inhomogeneity is also used for the study of the PRNU (flat field), but for relative radiometry in that case. Indeed, to obtain the PRNU, the signal of the FPA pixels under illumination must be corrected first by the inhomogeneity of this illumination. In that case, this signal of the FPA in ADU (Analog Digital Unit) must simply be normalized by the $H(x, y, \lambda)$ function.

2.8 Operation center of the facility

The automation of the facility operations reduce the need to enter in the ISO-5 area during a payload characterization, after its installation. The facility is equipped with Thermal and Optical Ground Support Equipment systems (TGSE and OGSE) which provide LabVIEW user-friendly interfaces to operate in real-time the security, thermal-vacuum and optical equipment. The TGSE continuously manages the thermal status and regulation of the payload and its mount, as well as monitors the vacuum level inside the VC[10]. Thanks to setpoints for nominal regulation as well as a dedicated alarms system in case of any unexpected event, the TGSE software combined to the security system of the facility, guarantee payload save operations. On the other hand, the OGSE offers an extended remote control of the opto-mechanical equipment, for example for the wavelength selection, the level of illumination and the readout of photodiodes. If synchronized with the FPU-GSE of the payload, quasi automated characterization can be performed, as it was the case for the MAJIS VIS-NIR campaign.

3. FACILITY VALIDATION FOR THE MAJIS PROJECT

3.1 Radiometric validation

Straylight rejection on the optical path

As presented in Section 2.2 for a NIR detector under test, it is mandatory to filter the photon flux along the optical path for wavelengths larger than 1.5 µm. This straylight rejection from emitters at room temperature must be efficient until the full cut-off of the detector. For the characterization of the MAJIS VIS-NIR FM detector, the facility was accordingly equipped with a customized Short Wave Pass Filter[43] (SWPF) avoiding thermal emission emerging from the viewport of the VC and items in front of the viewport. It offers a quasi-nominal transmission between 400 nm and 900 nm, followed by a large sample of twelve-peak transmission between 900 nm and 1400 nm. Two SWPF were superimposed to filter as much as possible the straylight produced by the undesirable photons flux between 1.5 µm and 2.65 µm. The high rejection finally obtained is illustrated in Figure 8.

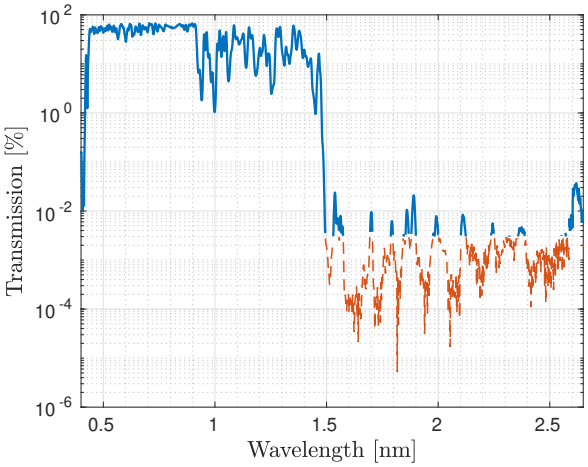

Figure 8. Transmission of the SWPF used for the MAJIS VIS-NIR project for straylight rejection of the optical path.

By modeling, it was demonstrated that the combination of both filters reduces the on-axis undesirable straylight on the MAJIS VIS-NIR detector to approximately 10 electrons per second (e^-/s), which could validates the use of a viewport even for VIS-NIR detectors characterization. However, additional off-axis straylight was observed during the MAJIS VIS-NIR FM characterization[11] and the FPU mount baffling will have to be improved for future tests. In that way, all characterization tasks (except the QE between 1.4 µm and 2.65 µm) using the 'diffuse' and 'converging' configuration beam were performed with a negligible impact of the straylight. For the QE characterization for wavelengths larger than 1.4 µm, the movable plate must be set in open position. The dynamical range is consequently reduced due to the level of straylight to be subtracted. Moreover, a shorter integration time must be used to avoid saturation by the straylight. Following this procedure, it is fully achievable to perform QE measurements.

Transfer function for absolute radiometry

The transfer function R_0 was determined for both configurations used during the MAJIS project. In that case, the FPA was aligned in a working plan fixed at a distance of 85 mm of the viewport. This function was built by using (i) the stable light source of the facility, (ii) VIS and NIR photodiodes coupled to a pinhole to represent dA, (iii) repetitive measurements of signal of these detectors alternately aligned on the IS reference port or a dedicated optical mount to represent the dA position.

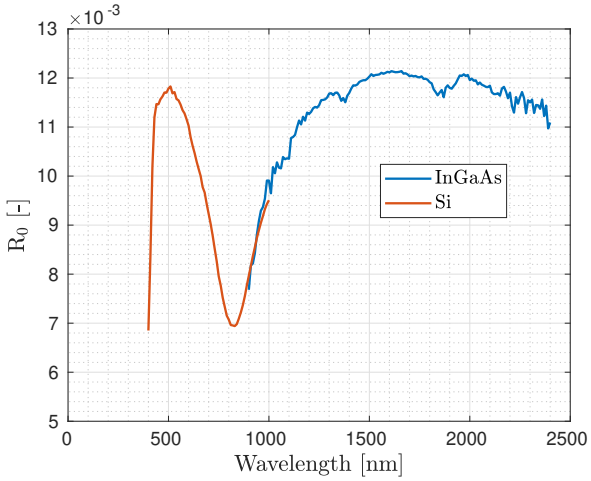

Figure 9. Spectral distribution of the transfer function R_0 as measured for the converging configuration of the facility.

R_0 was measured experimentally for all wavelengths covering the MAJIS VIS-NIR spectral range. One result of the validation campaign used to determine the transfer function R_0 is presented in Figure 9. The spectral dependence observed is mainly due to the spectral properties of the IS coating combined to some contribution related to the focusing array. Concerning the diffuse configuration (without the focusing array), the signal extinction between the FPA and the working plan is lower, by a factor of 10.

Homogeneity characterization in the working plan

The level of homogeneity in the working plan along a relative scale was characterized using a photodiode (Si for VIS, InGaAs for NIR) coupled with a pinhole, and mounted on a two-degree motorized (using actuators) translation system. Therefore under stable illumination, it was possible to scan the working plan and detect any illumination level variation. The scan step for the translation was set at 2 mm, followed by a numerical interpolation on a finer grid during the data processing (up to the pixel width of the VIS-NIR matrix detector). Repeated measurements were performed for wavelength sampling in the VIS-NIR spectral range. The propagation function $H(x, y, \lambda)$ could therefore be characterized, and normalized to one at the origin (coordinates (0,0)), corresponding to the intersection between the working plan and the facility optical axis. During the data processing, a negligible spectral dependence was observed. Consequently, it was proposed to proceed to the delivery of a unique matrix $H(x, y)$ after wavelength averaging. The results are presented in Figure 10 for a 24 mm $\times$ 24 mm surface, and interpolated every millimeter. The standard relative uncertainty associated to the function $H(x, y)$ is estimated at 2%. The expected circular symmetry of any inhomogeneity effect (the IS output port is circular) is well observed.

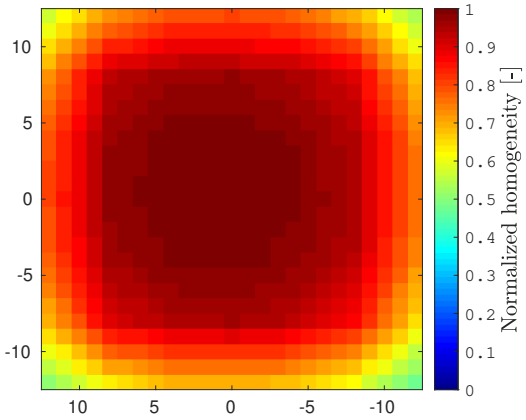

Figure 10. Characterization of the propagation function $H(x, y)$ for the diffuse configuration of the facility that describes the inhomogeneity in the working plan of the facility. The vertical and horizontal dimensions are in mm.

The propagation function homogeneity was also determined when using the focusing array between the IS and the viewport (linked to the MAJIS VIS-NIR project) in the same working area and with the same accuracy.

Level of illumination system and stability

The two filter wheels used for the MAJIS project include open and close position, and nine additional neutral density filters with different optical densities. They were selected in such a way that all cross combinations of filters contribute to a uniform sampling of the illumination level, from the maximum flux to a flux lowered by three to four orders of magnitude. Figure 11 shows that the first and second half of the available levels scan respectively the first order of magnitude, followed by the two others. Thanks to repetitive measurements with a well-linear photodiode at the IS level, the relative precision for one level of this relative flux scale is as good as 10^{-3} to 10^{-4}. This scale is generally used for linearity measurements in function of the flux, which is a non-wavelength dependent characterization. It is worth to mention that a slight wavelength change can offer a new set of 30 slightly different levels due to the spectral distribution of the QTH lamp combined to the spectrometer and fiber transmissions that are, obviously, wavelength dependent. Consequently, the facility can provide a quasi-infinite level of illumination.

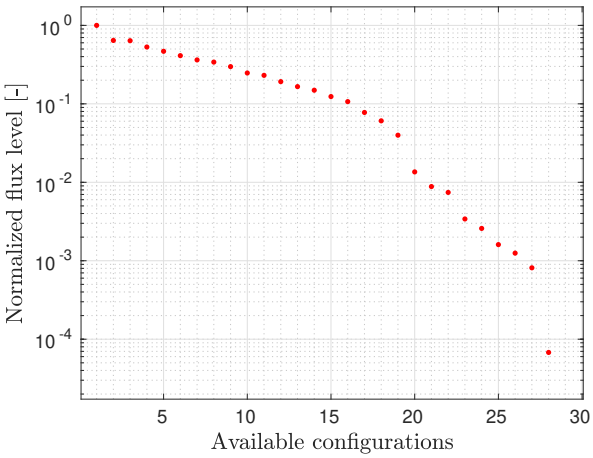

Figure 11. Distribution over three to four orders of magnitude of the level of illumination, using the filter wheels system of the facility.

Uncertainty for QE measurements

QE measurements are based on an equation using the spectral power $P(x, y, \lambda)$ as a variable. The combined standard uncertainty on P can be obtained from the derivative of Equation 2 . The respective uncertainties of the different measurands (right member of Equation 3) propagate to $P(x, y, \lambda)$, whose relative combined uncertainty can be expressed as follows:

$$\frac{\sigma QE}{QE} = \sqrt{\left(\frac{\sigma P_{IS}}{P_{IS}}\right)^2 + \left(\frac{\sigma R_0}{R_0}\right)^2 + \left(\frac{\sigma H}{H}\right)^2} \tag{3}$$

For this study, a simple case is presented. It starts with the determination of the transfer function R_0 during a pre-campaign, followed by the measurement of the spectral power $P_{IS}(\lambda)$ during a payload characterization campaign. For a given wavelength, this spectral power is the ratio between the photocurrent (A) of the photodiode ($S_{IS}(\lambda)$ in that case), and its calibration coefficient at this wavelength, called spectral power responsivity $C(\lambda)$, expressed in (A/W).

$$P_{IS}(\lambda) = \frac{S_{IS}(\lambda)}{C(\lambda)} \tag{4}$$

Thanks to repetitive measurements reducing uncertainty related to random (photon) noise, it was demonstrated that a photocurrent can be measured within 0.1 % of accuracy. For absolute measurements, the spectral range 400 nm - 1800 nm can be covered respectively by Si and Ge photodiodes, absolute calibrated by PTB. The certificates stated a relative standard uncertainty of 0.1 % for the Si detector. Concerning the Ge spectral coverage, this uncertainty is about 0.3 % to 0.4 % between 1000 nm and 1500 nm, and 1 % between 1500 nm and 1800 nm. The PbS photodiode (calibrated by Bentham) is used for wavelengths larger than 1.8 µm. The relative standard uncertainty is currently estimated at 5 % but will be improved using available standards of spectral irradiance, thanks to the BIRA-IASB and Bentham joint work. Using a quadratic mean, the uncertainty on $P_{IS}(\lambda)$ can be calculated, as reported in Table 1. The transfer function R_0 is a ratio of photodiode signals, also affected by the uncertainty related to the optical alignment of the photodiode at the intersection point between the optical axis and the working plan. The uncertainty of this ratio is therefore considered higher than a quadratic mean of 0.1 %, and adjusted instead to about 1 %. As stated previously, the uncertainty for the propagation function H is 2 %. Therefore, the resulting combined standard uncertainty for $P(x, y, \lambda)$ can now be calculated. The values obtained are summarized in Table 1.

Table 1. Estimation of the relative standard uncertainty of the measurands in the equation for absolute radiometry in the working plan, and combined results for the spectral power.

	Relative standard uncertainty (%)					
Spectral range (nm)	$\mathbf{C}(\lambda)$	$\mathbf{S_{IS}}(\lambda)$	$\mathbf{P_{IS}}(\lambda)$	$\mathbf{R_0}$	$\mathbf{H}(\mathbf{x},\mathbf{y})$	$\mathbf{P}(\mathbf{x},\mathbf{y},\lambda)$
400 - 1000	0.1	0.1	0.141	1	2	2.241
1000 - 1500	0.4	0.1	0.412	1	2	2.274
1500 - 1800	1	0.1	1.005	1	2	2.451
1800 - 2650	5	0.1	5.001	1	2	5.478

3.2 Thermal-vacuum validation

The cryogenic system of the facility reproduces the space conditions at which the MAJIS VIS-NIR detector will be exposed, and guarantees its cleanliness level and safety requirements[10]. The cryogenic system and TGSE were validated with the Structural Model (STM) and Engineering Model (EM) detectors. However, some iterative blank tests took place to improve the straylight rejection performances outside the optical path and to improve the warming-up stated procedure. The main purposes of the validation tests were: characterize the temperature difference between the FPA and the copper base plate, estimate the thermal dependence between the internal components of the FPU and the facility, characterize the thermal behavior of the radiation shield, characterize the required time to change the temperature of the FPA to detail the planning of measurements, and verify the temperature stability of the FPA. The security system was validated in parallel during the same thermal/vacuum tests[10].

During the STM validation campaign, the heat load of the FPU (including harnesses) was simulated by heaters located at the FPA and FPE, while temperature was monitored by different PT100 temperature sensors. The STM validation demanded an additional circuitry for thermometry, independent of the expected for the FM/SM detectors. The main tests consisted in characterize the behavior of the STM detector at different temperatures while simulating nominal power dissipation, and at different power dissipations while at operating temperature. Additionally, the STM validation tests probed the possibility to achieve a minimum temperature of 95 K in the copper base plate of the mount (no thermal load), with the cold head around 68 K. This represents the real low temperature limit of the facility. Usually the FPA is only about 3 K above the temperature of the copper base plate. However, the MAJIS VIS-NIR detectors were not exposed to such low temperatures since the characterization range was fixed above 125 K. On the other hand, thanks to the security system developed[10], the detectors were never under damage risk by low temperature. The STM campaign was limited due to the absence of FPF between the FPA and the FPE STM, so the real temperature dependency between both components could not be precisely characterized. Therefore, the most realistic test to accomplish this objective, was during the EM campaign.

For the EM validation campaign, PT100 temperature sensors were still installed on the FPU to verify the measurements by the Cernox temperature sensors at the FPA and FPE, which are intended to be used during the mission. The temperature difference observed between the FPA and the copper base plate was 3.8 K in average. Moreover, the real thermal coupling between the FPA and the FPE was well characterized for the different read-out modes of the detector. Figure 12 shows the unavoidable heating of the FPA through the FPF in a particularly observable region during measurements at different acquisition modes. As agreed, the temperature sensors of the FPU could not be used as elements of the thermal control loops[12]. Therefore, the PID parameters of the thermal control, to compensate these temperature changes in real time, were not modified. The solution proposed was to either compensate the temperature changes at copper plate level, or wait between image acquisitions until the temperature of the FPA recovers the expected temperature range ($\pm$0.5K). This situation also limited the use of the FPA at temperatures higher than 144 K, since in order to reduce additional noise in the images, they must be acquired with the FPE working below a temperature of 160 K. Therefore, the temperature characterization range (originally defined up to 160 K) was reduced accordingly. This situation is independent from the facility and could not be avoided.

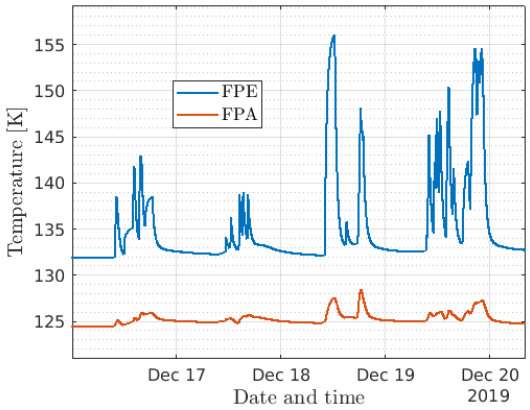

Figure 12. Thermal coupling between the FPE and the FPA, induced by the FPF during measurements; the temperature of the copper plate was stable. The high temperature increase observed on December 18, corresponds to the use of the high acquisition mode. The estimated amplification factor defined as the ratio between the temperature increase of the FPA and FPE is roughly around 10 % for the slow acquisition mode.

During the EM campaign, the level of straylight detected by the FPA was too high to validate the dark conditions of the facility (configuration 1) and therefore the facility was only validated for light measurements (configurations 2 and 3) and for training of the operators in image acquisition and use of the facility. The movable plate and SWPF achieved a minimum temperature of 195 K while simulating the FPA at operative temperature, which is not enough to avoid parasite radiation on the detector (only possible below 172 K). The blank tests performed before the delivery of the SM detector allowed the improvement of the setup to reduce the temperature of the shielding elements of the FPU. The final temperature achieved by the movable plate and the radiation shield, while simulating the hottest temperature of the FPA (144 K), was about 163 K and 148 K, respectively. The temperature of the movable plate could only approach the limit of 172 K if the FPA were at a temperature of 150 K. The thermal radiation produced by the movable plate on the detector was estimated as 9.3×10^{-3} e^-/pix for the nominal case, and 7.4×10^{-2} e^-/pix for the hottest case. On the other hand, the incident light from the viewport of the vacuum chamber inside the radiation shield, induces a temperature increment of all the elements inside the radiation shield. Unfortunately, this effect was not characterized during the EM campaign. Figure 13 shows the temperature changes observed in the elements that constitute the radiation shield when the movable plate is used in different configurations (close, open, filter). Note that when the movable plate is in open position, the temperature of the copper plate is also perturbed but thanks to the PID control loop, the oscillations are within 0.08 K and should not affect the stability of the FPA temperature. Nevertheless, it is expected that the FPU is also affected by the incoming light beam during different configurations. To avoid the FPA from varying its temperature outside its temperature range (±0.5 K), the same solution presented earlier to compensate the FPE thermal coupling, was proposed: either to compensate the temperature changes at copper plate level, or to wait until the temperature of the FPA recovers the expected temperature range after a change in the position of the movable plate. Since the temperature in the movable plate stabilizes around 2 hours after a position change, and the temperature increase should be simultaneous, a similar waiting time is expected for the stabilization of the temperature of the FPA.

Finally, the time-periods needed for the different phases of a characterization campaign were verified. For instance, at least 100 minutes are needed to achieve a vacuum level from room pressure to below 1×10^{-4} mbar in the vacuum chamber. Then, the cryocooler can be activated to start the cooling down process of the FPU. About 4 hours more are needed to stabilize the temperature of the copper plate in its operating range, with a rate of - 0.9 K/min. The FPU would stabilize its temperature about 2 hours later. Since the temperature of the movable plate (and other radiation shield components) remains below 172 K, it is not necessary to wait for its temperature stabilization to perform measurements; the thermal radiation that it provides to the detector is always negligible. As confirmed in the EM campaign, the FPU is never exposed to temperature changes faster than 5 K/min, as demanded by IAS[12].

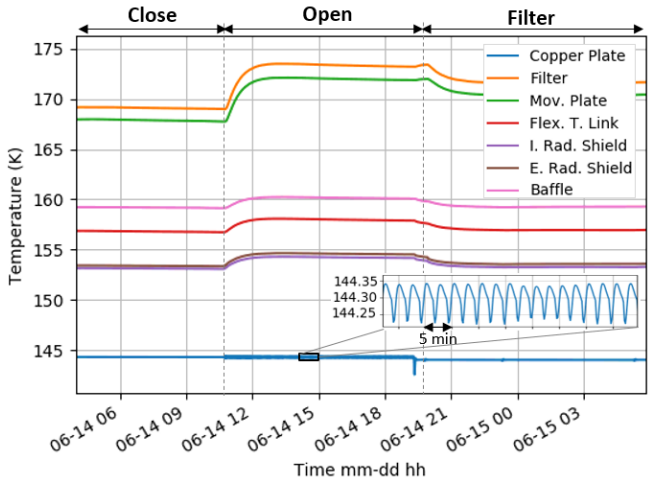

Figure 13. Temperature variations induced in the different components of the radiation shield when the movable plate changes position. A similar effect is expected in the FM FPU during its characterization. For this test, the copper plate was simulating the worst temperature case for the facility, so the movable plate overpasses by 1 K the temperature limit of 172 K in open position; the FPA would be around 150 K. It is not expected that the perturbations observed in the copper plate affect the stability of the temperature of the FPA during its characterization.

For the warming up of the FPU, it is intended to gradually increase the temperature of the FPU by steps of 10 K until the new temperature value, minding the temperature of the coldest item, to avoid molecular contamination on the FPU. To achieve room temperature, the cryocooler could be deactivated above a temperature of 200 K in the FPA, depending on the temperature evolution of the mount and the vacuum level of the VC. Figure 14 shows the vacuum and temperature evolution of the facility during the cooling down and warming up procedure of the mount (no FPU was installed inside the vacuum chamber). This information was useful to define the characterization planning for the FM campaign.

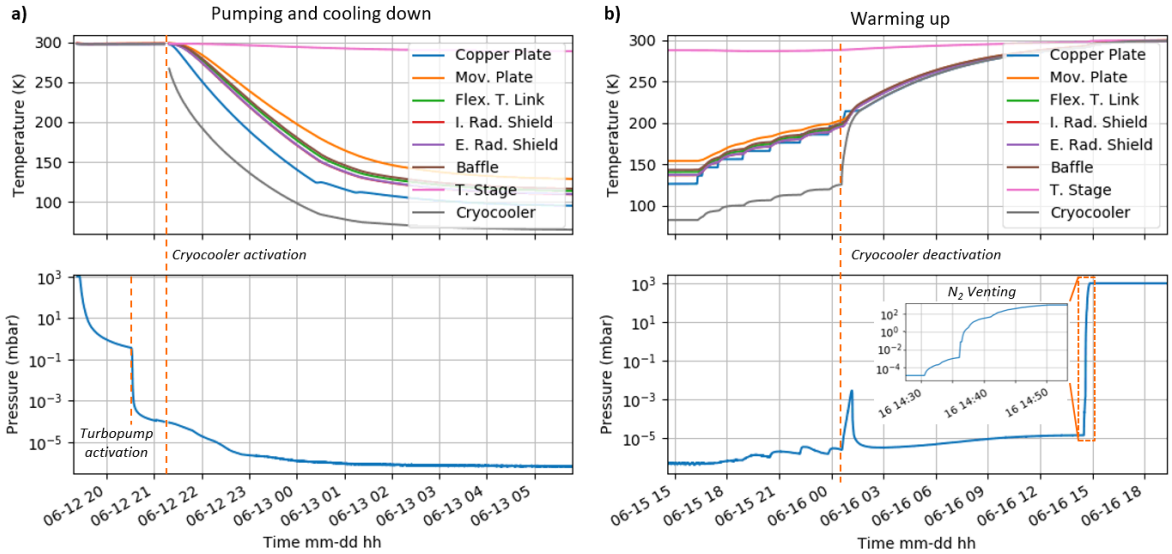

Figure 14. a) Pumping down of the vacuum chamber and coling down of the FPU mount, b) warming up of the FPU mount and N_2 venting of the vacuum chamber. This blank test allowed the characterization of the total waiting time to achieve the operating temperature of the FPA and the definition of the warming up process of the FPU. No FPU model was installed in the mount during this test.

4. CONCLUSIONS

BIRA-IASB and ROB institutes have more than thirty years of experience in space projects, for the development of instruments and their characterization in the field of solar physics, solar irradiance measurements and planetology. BIRA-IASB and ROB institutes, part of the STCL structure, provide facilities and expertise, namely to support the characterization of sub-systems for space instrumentation. For instance, the STCL contributes to the development of dedicated facilities with optimized performances in function of an ongoing space project. One recent objective was to increase the expertise in thermal-vacuum, for the electro-optical characterization of matrix detectors in the NIR. Since 2018, one opportunity had been offered by the MAJIS/JUICE project, through the Memorandum of Understanding (MoU) with IAS (France), for the FM and SM characterization of the VIS-NIR detectors. Therefore, a dedicated facility was developed for this project. The main equipment, installed in an ISO-5 area, is a large cubic vacuum chamber coupled to a cryo-cooling system. The cooling system is able to operate in the temperature range of 95 K to 160 K, although during the characterization of the MAJIS VIS-NIR detectors it was used between 125 K and 144 K. The optical equipment, external to the vacuum chamber, offers a stable monochromatic light beam, adjustable for central wavelength, bandwidth and level of illumination. The radiance can be transferred toward a working plan inside the vacuum chamber thanks to a CaF_2 viewport. The homogeneity of this illumination is well characterized and reproducible thanks to well-defined procedures for optical alignment. The illumination is provided in a diffuse or quasi-collimated configuration. Using calibrated photodiode and a measurement equation, the spectral radiant power can be calibrated for both configurations, for absolute radiometry. TGSE and OGSE software developed in LabVIEW, provide a quasi-fully automated control of the facility. In addition, a high-level security system developed at BIRA-IASB, is able to safely thermalize the MAJIS/JUICE VIS-NIR detectors without compromising any critical part of a payload. For the MAJIS VIS-NIR project, a special detector mount was designed to thermalize the detector according to the requirements, and to protect it against straylight contamination. This mount integrates a movable cold plate that allows a full set of characterization tasks in dark or under illumination conditions for a matrix VIS-NIR detector. The facility developed was used for the characterization of the FM VIS-NIR detector of the MAJIS instrument and the campaign took place at BIRA-IASB between end of June to beginning of September 2020. The only limitation of the facility performance concerns the QE measurements for wavelengths larger than 1.5 μm, for which the straylight on the optical path is less reduced. Outside the optical path, it was challenging to reject the straylight, but the facility reached quasi-nominal performances at the end of the campaign. The thermal-vacuum system developed at BIRA-IASB was fully certified to receive, operate and characterize the MAJIS VIS-NIR FM and SM detectors. Thanks to the versatility philosophy followed during the development of the calibration facility and its security system, its use for other projects is easily feasible, despite the need to slightly modify the mount that was especially developed for the MAJIS project. Full integrated instrumentation, as a small satellite, can also be characterized using this facility, in the VIS and NIR spectral ranges, for cryogenic and simulated space environment (10^{-6} mbar). An extension in the UV spectral range is under study.

ACKNOWLEDGMENTS

This project acknowledges funding, (i) by the Belgian Science Policy Office (BELSPO) by PRODEX-11 Project Proposal: *Characterization of JUICE/MAJIS VIS-NIR detectors* (PEA 4000124255); (ii) by the ESA JUICE Project; and (iii) by the Scientific Research Fund (FNRS) by the Aspirant Grant: 34828772 MAJIS detectors and impact on science.

REFERENCES

[1] Dominique, M., Hochedez, J. F., Schmutz, W., Dammasch, I. E., Shapiro, A. I., Kretzschmar, M., Zhukov, A. N., Gillotay, D., Stockman, Y., and BenMoussa, A., "The LYRA Instrument Onboard PROBA2: Description and In-Flight Performance," *Solar Physics* **286**, 21–42 (August 2013).

[2] BenMoussa, A., Giordanengo, B., Gissot, S., Meynants, G., Wang, X., Wolfs, B., Bogaerts, J., Schühle, U., Berger, G., Gottwald, A., Laubis, C., Kroth, U., and Scholze, F., "Characterization of Backside-Illuminated CMOS APS Prototypes for the Extreme Ultraviolet Imager On-Board Solar Orbiter," *IEEE Transactions on Electron Devices* **60**, 1701–1708 (August 2013).

[3] Bolsée, D., Pereira, N., Gillotay, D., Pandey, P., Cessateur, G., Foujols, T., Bekki, S., Hauchecorne, A., Meftah, M., Damé, L., Hersé, M., Michel, A., Jacobs, C., and Sela, A., "SOLAR/SOLSPEC mission on ISS: In-flight performances for SSI measurements in the UV," *Astronomy and Astrophysics* **600 A21** (2017).

[4] Mahieux, A., Berkenbosch, S., Clairquin, R., Fussen, D., Mateshvili, N., Neefs, E., Nevejans, D., Ristic, B., Vandaele, A. C., Wilquet, V., Belyaev, D., Fedorova, A., Korablev, O., Villard, E., Montmessin, F., and Bertaux, J.-L., "In-flight performance and calibration of SPICAV SOIR onboard Venus express," *Applied optics* **47**, 2252–2265 (2008).

[5] Neefs, E., Vandaele, A. C., Drummond, R., Thomas, I., Berkenbosch, S., Clairquin, R., Delanoye, S., Ristic, B., Maes, J., Bonnewijn, S., Pieck, G., Equeter, E., Depiesse, C., Daerden, F., Ransbeeck, E., Nevejans, D., Rodriguez-Gómez, J., Lopez-Moreno, J.-J., Sanz, R., and Jankowski, M., "NOMAD spectrometer on the ExoMars trace gas orbiter mission: Part 1 - design, manufacturing and testing of the infrared channels," *Applied Optics* **54**, 8494–8520 (2015).

[6] Langevin, Y., Pascal, E., Renotte, E., Gérard, J.-C., Karatekin, Ö., and Ann-Carine, V., "Memorandum of Understanding between IAS and CSL, ULiège, ROB and BIRA-IASB," (2015).

[7] Grasset, O., Dougherty, M., Coustenis, A., Bunce, E., Erd, C., Titov, D., Blanc, M., Coates, A., Drossart, P., Fletcher, L. N., et al., "JUpiter ICy moons Explorer (JUICE): An ESA mission to orbit Ganymede and to characterise the Jupiter system," *Planetary and Space Science* **78**, 1–21 (2013).

[8] Langevin, Y., Piccioni, G., and team, M., "MAJIS (Moons and Jupiter imaging spectrometer) for JUICE: objectives for the galilean satellites," in [*European Planetary Science Congress*], **8**, 548–1 (2013).

[9] Teledyne Imaging Sensors, *H1RG^{TM} Visible and Infrared Focal Plane Array* (2018).

[10] Cisneros-González, M. E., Bolsée, D., Van Laeken, L., Pereira, N., Gerard, P., Robert, S., Vandaele, A. C., Karatekin, Ö., Poulet, F., Dumesnil, C., Dubois, J. P., Hansotte, J., Le Du, M., and Picot, L., "Thermal-vacuum and security system of the characterization facility for the MAJIS/JUICE VIS-NIR FM and SM detectors," in [*Space Telescopes and Instrumentation 2020: Optical, Infrared, and Millimeter Wave*], **submitted**, International Society for Optics and Photonics (2020).

[11] Cisneros-González, M. E., Bolsée, D., Pereira, N., Van Laeken, L., Depiesse, C., Jacobs, L., Robert, S., Vandaele, A. C., Gissot, S., Karatekin, Ö., Poulet, F., Langevin, Y., Dumesnil, C., Dubois, J. P., Arondel, A., Haffoud, P., Ketchazo, C., Hervier, V., and Crane, B., "MAJIS/JUICE VIS-NIR FM and SM detectors characterization," in [*Space Telescopes and Instrumentation 2020: Optical, Infrared, and Millimeter Wave*], **submitted**, International Society for Optics and Photonics (2020).

[12] MAJIS Team, "MAJIS FPU VIS-NIR Requirement Specifications," tech. rep., Institute of Space Astrophysics (IAS) (2018). Ref: JUI-IAS-MAJ-RS-021.

[13] Pfeiffer Vacuum, *DN-750 TrinosLine High-Vacuum Chamber, Cubical.*

[14] Pfeiffer Vacuum, *HiPace 300 H Turbopump* (2018).

[15] Pfeiffer Vacuum, *ACP 15, Standard, three phase, manual gas ballast* (2018).

[16] Pfeiffer Vacuum, *PKR-361 Compact Full-Range Gauge* (2015).

[17] Pfeiffer Vacuum, *MPT-200 Digital Pirani/Cold Cathode Gauge* (2015).

[18] ARS Closed Cycle Cryocoolers, *Model CS104FT* (2010).

[19] Van Laeken, L., *Development of experimental benches for radiometric characterization: Application to space instrument MAJIS VIS-NIR on JUICE.*, Master's thesis, Université de Liège, Liège, Belgium (2019). https://matheo.uliege.be/handle/2268.2/8417.

[20] PAR Group Ltd, "Technical data sheet."

[21] LakeShore, *Model 335 Temperature Controller* (2017).

[22] LakeShore, *Model 336 Temperature Controller* (2017).

[23] LOT Quantum Design, *QTH 1000 W.*

[24] Keysight Technologies, *HP 6675A Single-Output,2000 W DC Power Supplies, GPIB* (2019).

[25] LOT Quantum Design, *Arc light sources 450-1200W.*

[26] Bentham Instruments Limited, *218M Optical Chopper & Control Module* (2020).

[27] Uniblitz, *35mm Bi-Stable Optical Shutter datasheet, DSS335B* (2017).

[28] Bolsée, D., *Métrologie de la spectrophotométrie solaire absolue. Principes, mise en oeuvre et résultats. Instrument SOLSPEC à bord de la Station Spatiale Internationale.*, PhD thesis, Free University of Brussels, Brussels, Belgium (2012). http://difusion.ulb.ac.be/vufind/Record/ULB-DIPOT:oai:dipot.ulb.ac.be:2013/209709/Holdings.
[29] Bentham Instruments Limited, *DTMc300 Double-monochromator with triple grating turret.*
[30] Newport Inc., *819D-IS-5.3 Spectralon Diverging Beam Integrating Spheres* (2017).
[31] Bentham Instruments Limited, *FOP Series. IR-4-1000 fiber Optic Bundles.*
[32] Bentham Instruments Limited, *DH-Si Silicon Detector* (2018).
[33] Newport Inc., *Germaniumflange mount photodiode sensor, 71653, 700-1800 nm* (2017).
[34] Bentham Instruments Limited, *DH-PbS-Te Cooled Lead Sulphide Detector* (2018).
[35] Hamamatsu Photonics, *Infrared detector module with preamp, C12486-210* (2017).
[36] Keysight Technologies, *34970A Data Acquisition/Switch Unit Family* (2020).
[37] Tektronix, *Keithley Series 6485 Picoammeters* (2020).
[38] Bentham Instruments Limited, *496 DSP Lock-In Amplifier* (2020).
[39] Bentham Instruments Limited, *477 AC Current Pre-Amplifier* (2020).
[40] Lambda-X, "MAJIS-RP-LX-0001 Optical Design Report," tech. rep., Lambda-X (2019). Ref: MAJIS-RP-LX-2019-01.
[41] Werner, Lutz and Vogel, Katrin, "Optischer Strahlungsdetektor mit einer Sillizium-Photodiode / Optical radiation detector with silicon photodiode," tech. rep., Physikalisch-Technische Bundesanstalt (PTB), Berlin (2019). Ref: 7.3-1.25-18-30.
[42] Werner, Lutz and Vogel, Katrin, "Optischer Strahlungsdetektor mit einer Germanium-Photodiode / Optical radiation detector with germanium photodiode," tech. rep., Physikalisch-Technische Bundesanstalt (PTB), Berlin (2019). Ref: PTB-7.3-1.25-19-05.
[43] Northumbria Optical Coatings, *Short Wave Pass Filter NOC_SWPF_CertificateAndTransmission77K, NC 2065(D)* (2020).

APPENDIX A. ACRONYMS

BELSPO	Belgian Science Policy Office
BIRA-IASB	Royal Belgian Institute for Space Aeronomy
CNES	National Centre for Space Studies
DC	Dark Current
DSNU	Dark Signal Non-Uniformity
ESA	European Space Agency
EUV	Extreme UltraViolet wavelength range
FM	Flight Model
FNRS	Scientific Research Fund
FPA	Focal Plane Array
FPE	Focal Plane Electronics
FPU	Focal Plane Unit
FWC	Full Well Capacity
GSE	Ground Support Equipment
IAS	Institute of Space Astrophysics
IR	InfraRed wavelength range
IT	Integration Time
JUICE	JUpiter Icy Moons Explorer
LVF	Linear Variable Filter
MAJIS	Moons And Jupiter Imaging Spectrometer
MLI	Multi-Layer Insulation
NIR	Near-InfraRed wavelength range
OFHC	Oxygen-Free High Conductivity
OGSE	Optics Ground Support Equipment
PEA	Prodex Experiment Arrangement
PID	Proportional-Integral-Derivative
PRNU	Photo Response Non-Uniformity
PTB	Physikalisch-Technische Bundesanstalt
QE	Quantum Efficiency
QTH	Quartz Tungsten Halogen
ROB	Royal Observatory of Belgium
RON	Read-Out Noise
SAM	Secure Access Module
SM	Spare Model
STCL	Space optoelectronic and optical Technology and Calibration Laboratory
SWPF	Short Wave Pass Filter
TGSE	Thermal Ground Support Equipment
VC	Vacuum Chamber
VIS	VISible wavelength range